

# Glueballs and the superfluid phase of Two-Color QCD

M.P. Lombardo<sup>1</sup>, M.L. Paciello<sup>2</sup>, S. Petrarca<sup>2,3</sup>, and B. Taglienti<sup>2</sup>

<sup>1</sup> INFN, Laboratori Nazionali di Frascati, via E. Fermi 40, I00044 Frascati, Italy

<sup>2</sup> INFN, Sezione di Roma, P.le A. Moro 2, I-00185 Roma, Italy

<sup>3</sup> Dipartimento di Fisica *Sapienza* Università di Roma,  
P.le A. Moro 2, I-00185 Roma, Italy

the date of receipt and acceptance should be inserted later

**Abstract.** We present the first results on scalar glueballs in cold, dense matter using lattice simulations of two color QCD. The simulations are carried out on a  $6^3 \times 12$  lattice and use a standard hybrid molecular dynamics algorithm for staggered fermions for two values of quark mass. The glueball correlators are evaluated via a multi-step smearing procedure. The amplitude of the glueball correlator peaks in correspondence with the zero temperature chiral transition,  $\mu_c = m_\pi/2$ , and the propagators change in a significant way in the superfluid phase, while the Polyakov loop is nearly insensitive to the transition. Standard analysis suggest that lowest mass in the  $0^{++}$  gluonic channel decreases in the superfluid phase, but these observations need to be confirmed on larger and more elongated lattices. These results indicate that a nonzero density induces nontrivial modifications of the gluonic medium.

**PACS.** 12.38 Gc Lattice QCD calculations – 11.15.Ha Lattice gauge theory – 12.38.Aw General properties of QCD

## 1 Introduction

The study of the phases of QCD has applications to a wide array of subjects, ranging from heavy ion collision from FAIR to RHIC to LHC energies, the physics of compact stars, QCD phase transitions in the early universe, and more theoretical scenarios in which strongly coupled gauge theories might serve as a laboratory for physics beyond the standard model [1].

Lattice field theory provides a solid computational framework for these studies, in all those cases in which the determinant is positive and importance sampling can be applied. Unfortunately, at high baryon density the weight of the functional integral is complex, which forbids the usage of simple importance sampling in the computation.

At high temperature strong fluctuations of the baryon number makes it possible to study the physics of nonzero baryon density, and in this way we can explore the portion of the phase diagram which is analytically connected with the zero density quark gluon plasma region. Unfortunately, this excludes many different other phases of QCD, which appear at low temperatures and higher densities, see e.g. [2] for an overview.

Two color QCD is an important exception: the color SU(2) group in the fundamental representation is pseudo-real and in this case the determinant is real even when  $\mu \neq 0$  and standard hybrid Monte Carlo simulations are possible. So lattice calculations can confront and extend fermionic model studies [3].

However, very little happened in the field after the pioneering studies of the 80's [4, 5, 6]. The subject was revived after the work of the late 90's [7, 8]: these authors noted that phenomena associated by diquark condensations at high density might well be much more important than previously thought, if one goes beyond one gluon exchange when calculating the relevant four fermion couplings. Two color QCD was then reconsidered as a laboratory for a toy study of diquark condensation mechanisms [9]. Symmetries and spectrum were analysed in a quantitative way, and lattice studies of diquark condensation were carried out [10, 11]. Further studies include RMT analysis [12, 13] and studies of the Dirac spectrum [14]. Moreover, the fact that  $\mu_c(T=0) = m_\pi/2$  makes the model amenable to a  $\chi$ PT analysis [15]. In turn, chiral perturbation theory motivated studies produced results for the EoS and Gluon Condensate [16]. The model (with adjoint fermions) has been also used as a laboratory for the study of new universality classes [17]. The phase diagram has been computed in the chiral limit by use a new cluster algorithm [18]. Model studies of the vector sector [19] prompted studies of vector spectroscopy on the lattice [20, 21, 22, 23].

In short summary, model analysis, chiral perturbation theory, and the feasibility of lattice calculations conspired to make the fermionic sector of two-color QCD reasonably well understood, with numerical results in quantitative agreement with analytic calculations.

In comparison with the fermionic sector, the gluodynamics of two-color QCD is much less well known. Stud-

ies have been carried over at high temperature, where the finite  $\mu$  transition is similar to the one at finite  $T$  [25,26], while at low temperature the behaviour of the Polyakov loop and of the gluon propagator indicates that the hadronic/superfluid transition and the deconfining transition are well separated phenomena [27].

In this study we present a quantitative analysis of the scalar plaquette-plaquette correlator, with the main goal of making progress on our understanding of the phase diagram of QC<sub>2</sub>D at low temperature, and to get further insight into the nature of the gauge field dynamics at high baryon density, in a region which is distinctly different from the ordinary, high temperature, high baryon density phase. Glueballs have been considered as probes of the thermal medium in [28,29].

Previous work on the subject has discussed at length the similarities and differences between the phase diagrams of two and three colors QCD. In short, while the properties of the matter above  $T_c$  are substantially independent on the number of colors the nature of the low temperature, high density phase seems to depend strongly on the number of colors. At the same time, though, many of the differences appear in the fermionic sector, where different couplings produce different pattern of the symmetries realisation. The gluonic sector is not directly related with these different symmetries, and might well exhibit characteristics independent on the number of colors. This is one of the motivation for a lattice study. On a more general grounds, two color QCD at high density affords an example, as we will see, of a chiral transition clearly separated from the deconfining one.

This paper is organized as follows: in the next Section we review a few basic facts about two color QCD and its phase diagram; Section 3 is devoted to the details of the simulations, while Section 4 deals with observables and measurement strategies. Smearing [33] is introduced and reviewed there. Section 5 contains the results: we discuss the behaviour of the scalar gluonic correlators constructed by the smearing technique in order to excite glueballs and study their behavior as a function of baryon density. Results for the Polyakov loop are presented as well. In Section 6 we summarise and discuss our findings, and outline future research.

A preliminary account of some of the results have appeared in [30,31].

## 2 Action, symmetries, phase diagram

Let us briefly remind here a few features of the thermodynamics of the two color model on which we will rely in the following. The above mentioned reviews and literature can of course be consulted for more details.

The lattice version of the Action reads [9]:

$$S_{kin} = \sum_{x, \nu=1,3} \frac{\eta_\nu(x)}{2} [\bar{\chi}(x) U_\nu(x) \chi(x + \hat{\nu}) - \bar{\chi}(x) U_\nu^\dagger(x - \hat{\nu}) \chi(x - \hat{\nu})] + \sum_x \frac{\eta_t(x)}{2} [\bar{\chi}(x) e^\mu U_t(x) \chi(x + \hat{t}) - \bar{\chi}(x) e^{-\mu} U_t^\dagger(x - \hat{t}) \chi(x - \hat{t})]$$

where a chemical potential per quark was introduced in the usual way [4,32].

At  $\mu = 0$  the Action enjoys the lattice equivalent of Pauli-Gürsey symmetry:

$$\tau_2 U_\mu \tau_2 = U_\mu^* \quad (1)$$

where  $\tau_2$  is Pauli matrix .

The Action can be recast

$$S_{kin} = \sum_{x \text{ even}, \nu=1,3} \frac{\eta_\nu(x)}{2} [\bar{X}_e(x) U_\nu(x) X_o(x + \hat{\nu}) - \bar{X}_e(x) U_\nu^\dagger(x - \hat{\nu}) X_o(x - \hat{\nu})] + \sum_{x \text{ even}} \frac{\eta_t(x)}{2} [\bar{X}_e(x) \begin{pmatrix} e^\mu & 0 \\ 0 & e^{-\mu} \end{pmatrix} U_t(x) X_o(x + \hat{t}) - \bar{X}_e(x) \begin{pmatrix} e^{-\mu} & 0 \\ 0 & e^\mu \end{pmatrix} U_t^\dagger(x - \hat{t}) X_o(x - \hat{t})]$$

with the definitions

$$\bar{X}_e = (\bar{\chi}_e, -\chi_e^{tr} \tau_2) \quad : \quad X_o = \begin{pmatrix} \chi_o \\ -\tau_2 \bar{\chi}_o^{tr} \end{pmatrix}. \quad (2)$$

which make even more transparent the equivalence of quarks and antiquarks in the model.

At  $\mu = 0$  The (Pauli-Gürsey) symmetry implies the degeneracy of mesons and baryons (diquarks) with opposite parities:

$$m_\pi = m_{qq} \quad (3)$$

In turn, this produces only one discernible condensate,  $\langle \bar{\psi} \psi \rangle^2 + \langle \psi \psi \rangle^2$ , whose direction is chosen by the mass term.

Consider now the thermodynamics of the model.

At zero density, high temperature there is a transition separating the ordinary hadronic phase from a quark gluon plasma. The characteristics of the high temperature and low temperature phases seem to be fairly independent on the number of colors, with  $T_c$  of the order of a typical mass scale (of course the precise nature of the transition is not). This remains true for a nonzero chemical potential, till the temperature if “high enough”, most likely till the transition is between a hadronic phase and a quark gluon plasma phase.

At zero temperature standard arguments indicate that there is no Fermi sea until the quark chemical potential exceeds the mass of the lowest state which carries baryon number, i.e half the mass of the baryon which is degenerate with the pion:  $\mu_c = m_\pi/2$ . For  $\mu > \mu_c$  the attractions

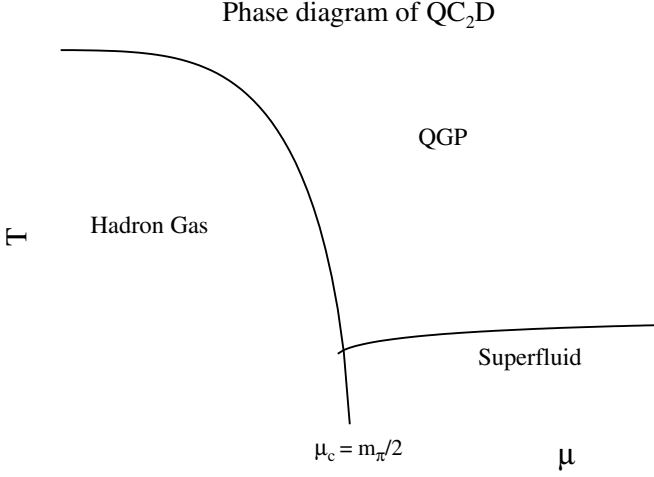


**Fig. 1.** Sketchy view of the phase diagram of two color QCD: we recognize (at least) three phases. A Hadronic phase, a BEC phase, and a Quark Gluon Plasma phase. The phases are characterised by the values of the  $\langle \bar{\psi}\psi \rangle$  and  $\langle \psi\psi \rangle$  condensates, the Polyakov loop and the number density. (In this plot we do not distinguish between transition and crossover lines)

in the diquark channel leads to the formation of a diquark condensate  $\langle \psi\psi \rangle$ . For two color QCD  $\langle \psi\psi \rangle$  is color neutral, like the chiral condensate itself: when  $\mu$  exceeds  $\mu_c$ ,  $\langle \bar{\psi}\psi \rangle$  rotates to  $\langle \psi\psi \rangle$ , and numerical simulations nicely follow the prediction of chiral perturbation theory for the chiral condensate, mass spectrum and thermodynamics.

### 3 The simulation

The simulations were performed using a standard hybrid molecular dynamics algorithm for staggered fermions using the same code as of ref. [9], which corresponds to  $N_f = 8$  continuum flavors.

Details on relevant parameters are summarised in table 1. Smaller  $dt$  were needed in the supercritical region and trajectory lengths ranged in most cases from half to one.

**Table 1.** Simulation parameters

lattice size	$6^3 \times 12$
$\beta$	1.3
configurations	40000
sweeps	10
$dt$	0.05 - 0.02
thermalization	1000 configurations
quark mass $m_q$	.05, .07
chemical potential $\mu$	.0, .2, .25, .30, .32, .35, .4, .6, .9
smearing weights $\omega$	.025, .05, .07, .1, .2, .3, .4
smearing steps	1, 2, 3, 4

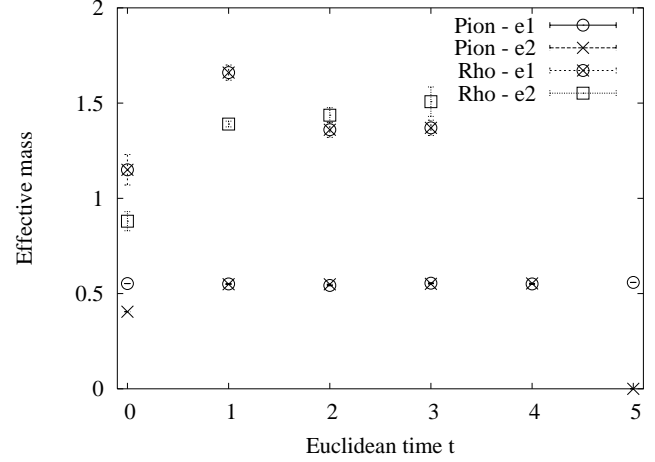


**Fig. 2.** Effective masses for the  $\rho$  and the  $\pi$  mesons in the normal phase ( $\mu = 0.0$ ) and bare quark mass  $m_q = 0.05$ , from the two different procedures labeled as e1 and e2, see text.

Values  $\mu = 0.25, 0.30, 0.32, 0.35, 0.90$  were simulated only at  $m_q = 0.07$ , with a slightly reduced statistics of 30000 steps. For the analysis we used a bin size of 7000, for which the errors level off.

To set the scale, we have measured the fermionic spectrum at  $\mu = 0.0$ .

We have constructed the zero momentum propagators  $C(t)$  for the pion and the  $\rho$  mesons in the standard way, assumed the form

$$C(t) = A \cosh[m(t - N_t/2)] \quad (4)$$

which is valid for euclidean times  $N_t$  larger than the reciprocal of the excited masses, and used two different definition of the (time dependent) effective masses  $m_{eff}(\bar{t})$ , one exploiting  $C(t)/C(t+1)$

$$C(\bar{t})/C(\bar{t}+1) = \frac{\cosh[m_{eff}(\bar{t})(\bar{t} - N_t/2)]}{\cosh[m_{eff}(\bar{t})(\bar{t}+1 - N_t/2)]} \quad (5)$$

the other  $C(t)/C(t+2)$ , according to

$$C(\bar{t})/C(\bar{t}+2) = \frac{\cosh[m_{eff}(\bar{t})(\bar{t} - N_t/2)]}{\cosh[m_{eff}(\bar{t})(\bar{t}+2 - N_t/2)]} \quad (6)$$

We show the results for the  $\rho$  and the pion at  $m_q = 0.05$ , in Fig. 2, where we label the effective masses extracted by use of the two definitions as e1 and e2 respectively. The two procedures give comparable results on a moderate range of times, indicating that the oscillatory contribution for the opposite parity partner, if any, is very small.

From the plateaus in the plots we read off  $m_\pi = 0.56(2)$  and  $m_\rho = 1.4(1)$ . A similar analysis at  $m_q = 0.07$  gives  $m_\rho = 1.5(2)$  and  $m_\pi = 0.64$ . In both cases  $m_\rho$  and  $m_\pi$  are well resolved, meaning that we are still within the range of chiral perturbation theory.

## 4 Glueball measurements: operators and smearing

The operators commonly used for measuring scalar gluonic correlators exciting glueball masses are Wilson loops. For simplicity we restricted ourselves to plaquette-like operators that can be built from four links.

Simple glueball wave functions such as the plaquette have the disadvantage that they only have small overlaps with the lowest-lying glueball states, and that these overlaps become rapidly smaller as the lattice spacing is decreased.

Furthermore the plaquette couples strongly to ultra-violet fluctuations, increasing the noise in the correlators; to have reliable glueball correlation functions at different distances, it is mandatory to reduce these statistical fluctuations.

Different smoothing procedures aimed at removing the unphysical short-distance fluctuations have been introduced; a short review can be found in [37]. One of this is the smearing method, originally proposed for SU(3) in [33]. It consists in the construction of correlation functions for operators which are a functional of the field smeared in space and not in time.

For each link  $U_\mu(x)$  of a configuration the product of the other three links defining a plaquette is considered, then these products are summed over the four choices of plaquettes orthogonal to the time axis; the resulting matrix is added with a weight  $w$  to the original link  $U_\mu(x)$ . This linear combination, projected back on the gauge group, is assumed as new link variable (the so called “fat link”). The procedure can be iterated, say  $N_s$  times.

This operation both enlarges the “size” of the ordinary plaquette operator and reduces the noise associated with the additional degree of freedom due to the gauge invariance. Only spatial links participate on the averaging. Thus the transfer matrix for the smeared operators is unaffected and it remains positive definite, if this was the case. The values of the smearing coefficient  $w$  and the number of iterations  $N_s$  are tuned in order to optimise the performance of the method [34,35,36].

The glueball operators are defined by means of the plaquettes  $P_{ij}(\mathbf{x}, t)$  on  $ij$  plane as in the following:

$$\phi^{0^{++}}(t) = \text{tr} \sum_{\mathbf{x}} \left[ P_{12}(\mathbf{x}, t) + P_{23}(\mathbf{x}, t) + P_{13}(\mathbf{x}, t) \right] \quad (7)$$

which transforms according to the  $A_1^{++}$  (one-dimensional) irreducible representations of the of the relevant cubic point group (on a lattice the full rotational symmetry is broken down to only cubic symmetry), and

$$\phi_a^{2^{++}}(t) = \text{tr} \sum_{\mathbf{x}} \left[ P_{12}(\mathbf{x}, t) - P_{13}(\mathbf{x}, t) \right] \quad (8)$$

$$\phi_b^{2^{++}}(t) = \text{tr} \sum_{\mathbf{x}} \left[ P_{12}(\mathbf{x}, t) + P_{23}(\mathbf{x}, t) - 2P_{13}(\mathbf{x}, t) \right] \quad (9)$$

which transform both according to the  $E^{++}$  (2-dimensional) representation. Note that all operators are projected onto zero momentum by averaging over all spatial sites.

These operators are the lattice counterparts of the continuum  $O(3) \otimes Z(2)$ ,  $J^{PC} = 0^{++}$  and  $2^{++}$  respectively. Hence, we can label the corresponding excitations as  $0^{++}$  and  $2^{++}$  states. Of course this correspondence is not one to one but infinite to one. What is usually measured is the lowest excitation in the corresponding representation of the cubic group, corresponding to the fundamental glueball state.

Unfortunately, but not unexpectedly, the  $2^{++}$  results turned out to be too noisy to provide any significant information. Because of this, we will base the following analysis on the  $0^{++}$  results alone.

With dynamical quarks, as in our case, mixing is possible between purely gluonic and fermionic operators. So strictly speaking we should not talk about “glueball masses”, but, rather, of the lowest excitation in that particular channel, be it fermionic, gluonic or a mix of the two. This said, for the sake of brevity, in the following we will sometimes speak of “glueballs”, meaning what has just been explained.

Following the methods previously depicted, a smeared operator is obtained replacing the ordinary link variables  $U(x)$  in the plaquette operator  $P_{ij}(\mathbf{x}, t)$  by the fat link  $U'(x)$ . Higher levels of smearing are obtained by varying the weight  $w$  and by iterating the procedure  $N_s$  times.

Glueball masses are calculated from the Euclidean time behaviour of their correlation functions:

$$C^{0^{++}}(t) = \frac{1}{N_t} \sum_{\tau=0}^{N_t-1} ( \langle \phi^{0^{++}}(\tau+t) \phi^{0^{++}}(\tau) \rangle - \langle \phi^{0^{++}}(\tau) \rangle^2 ) \quad (10)$$

where we exploited the cluster property

$$\lim_{t \rightarrow \infty} \phi^{0^{++}}(\tau+t) \phi^{0^{++}}(\tau) = \phi^{0^{++}}(\tau)^2 \quad (11)$$

as well as the translational invariance of  $\phi^{0^{++}}(\tau)$ . In the following whenever no confusion could arise we will refer to the propagator eq.10 simply as  $C(t)$ .

We have analysed the glueball correlations for different smearing parameters. One observation which allows a more compact analysis, as well as offers more control on the results, was proposed in ref. [35]. There, it has been shown that the two-dimensional parameters space of the number of sweeps  $N_s$  and the smearing weight  $w$  may be reduced to a single dimension via the parameter  $T_s = N_s \times w$ , in a certain range  $0 \leq w \leq w^{max}$ ,  $0 \leq N_s \leq N_s^{max}$ , where  $w^{max}$  and  $N_s^{max}$  depend, of course, on the specific application under consideration.

In our case, we have observed that the unidimensional parametrisation remains true till  $w \leq 0.3$ , irrespective of the number of smearing steps, at least within the allowed range of smearing steps  $N_s \leq S/2$ , where  $S$  is the spatial size of the lattice. Fig. 3 demonstrates this property in the normal ( $\mu = 0.0$ ) and in the superfluid phase ( $\mu = 0.6$ ) for the amplitude  $C(0)$  of the correlators built for our smallest quark mass  $m_q = 0.05$ . We have observed that

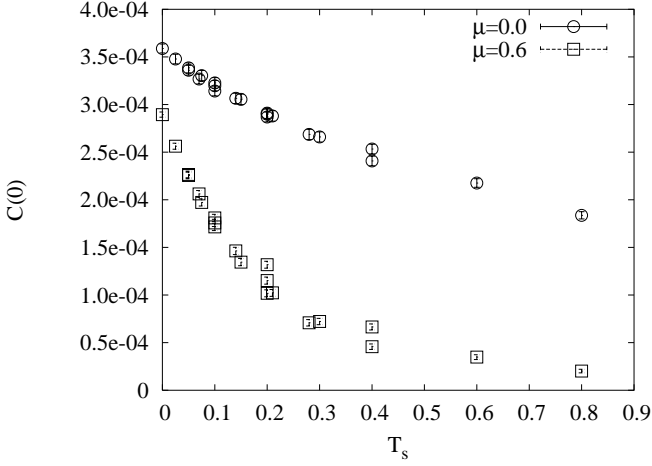


**Fig. 3.** Amplitude of the  $0^{++}$  correlator for smearing weight  $w$  and smearing steps  $N_s$  as a function of the smearing parameter  $T_s = N_s w$ , in the normal ( $\mu = 0.0$ ) and superfluid phase ( $\mu = 0.6$ ), for  $m_q = 0.05$ . Note the universal behaviour as a function of  $T_s$  in the two phases. Note also that smearing affects the results at  $\mu = 0.6$  more than those at  $\mu = 0.0$

this behaviour holds true also for other observables, and mass  $m_q = 0.07$ .

To be on the safe side, we will base our discussions on results within the range of validity of the unidimensional parametrisation: in conclusion,  $w \leq 0.3$ ,  $N_s \leq 3$ .

The same Fig. 3 allows a comparison of the effects of smearing in the two phases: we note that the smeared results drop much faster as function of  $T_s$  after the transition ( $\mu = 0.6$ ) than in the normal phase ( $\mu = 0.0$ ). We will come back to this point in the next section.

## 5 Results

We devote this Section to the presentation of the results for the glueballs and the Polyakov loop.

The raw results for the plaquette correlators

$$P(t) = \frac{1}{N_t} \sum_{\tau=0}^{N_t-1} \langle \phi^{0^{++}}(\tau+t) \phi^{0^{++}}(\tau) \rangle \quad (12)$$

for our smaller mass  $m_q = 0.05$  are presented in Fig. 4. The results in the two phases, the normal phase at  $\mu = 0.0$  and the superfluid phase,  $\mu = 0.4, 0.6$ , show the expected long distance plateaux.

This suggests to base our analysis on the propagators defined in eq. 10. However we will also consider the plaquette correlators eq. 12, which will require leaving the vacuum contribution as a fitting parameter.

The latter - fits to the plaquette correlators - will be our only analysis in the case of the critical propagators, since they show a peculiar behaviour, which we will describe a bit more fully at the end of this Section.

To get a first feeling about the results in the two phases we plot in Fig. 5 the  $0^{++}$  glueball correlators (eq.10), for

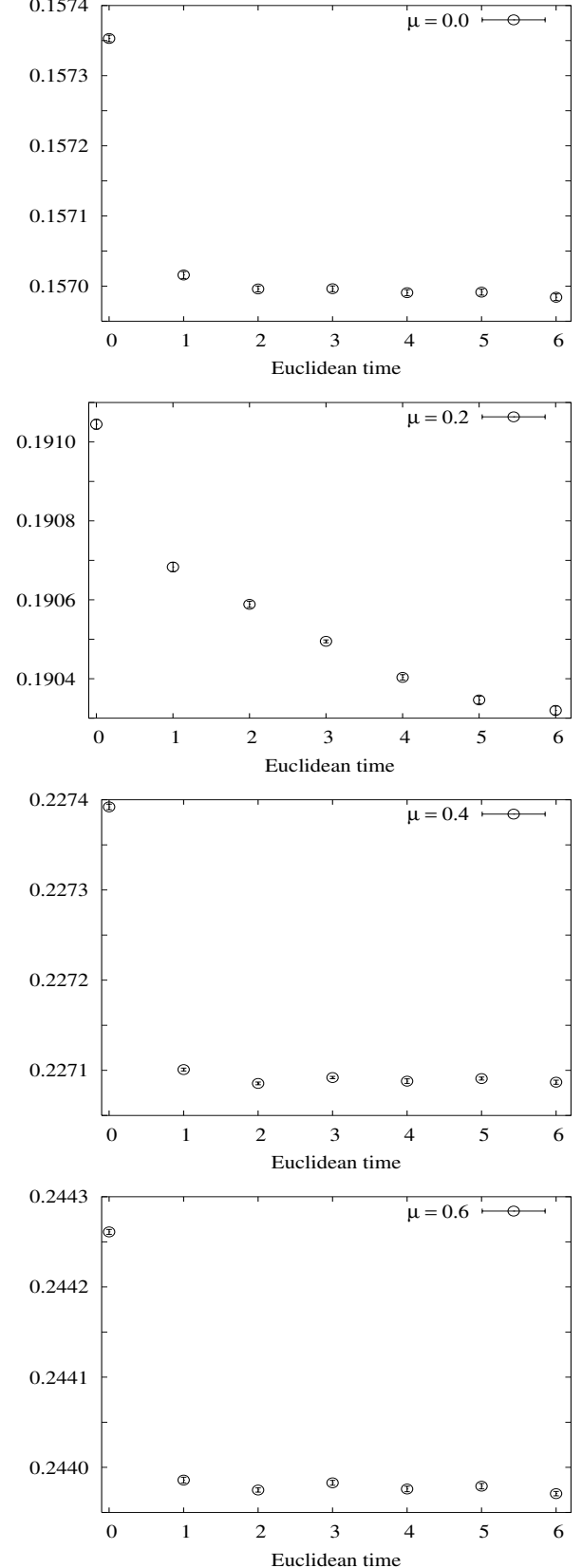


**Fig. 4.** Plaquette correlators (eq.12) at mass  $m_q = 0.05$  for a few  $\mu$  values.  $\mu = 0.2$  is close to the critical point, the two larger  $\mu$  are in the superfluid phase.

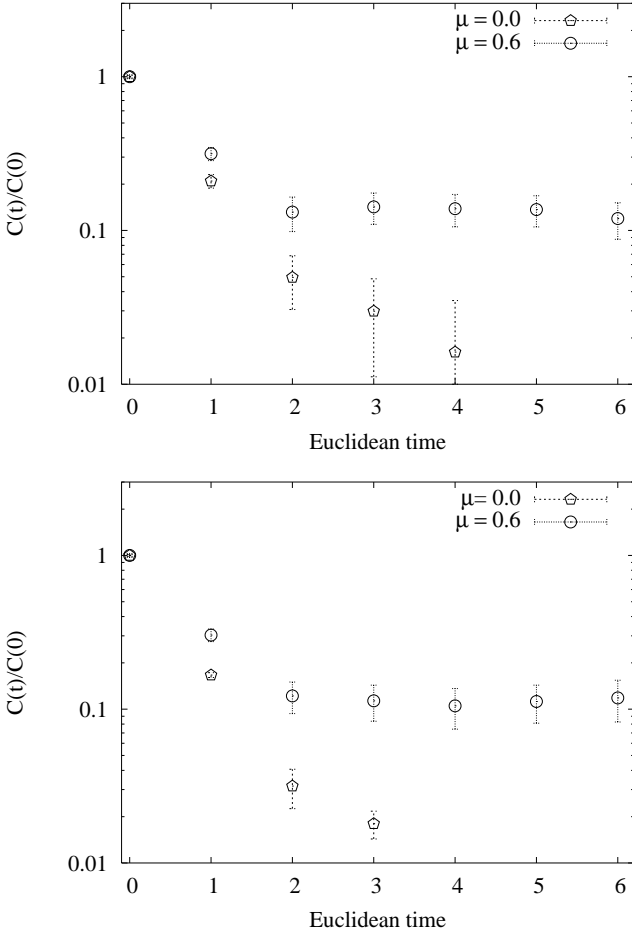


**Fig. 5.** Propagators of the scalar glueball at mass  $m_q = 0.05(0.07)$ , upper (lower) in the normal and superfluid phase, for smearing parameters  $w = 0.3, T_s = 1$ , normalised to one at zero distance. Either diagrams demonstrate the decrease of the mass of the lowest excitation in the scalar glueball channel when going from the normal to the superfluid phase.

the two masses we have inspected, smearing parameters as indicated, and for the two phases. Other smeared data behave similarly. We normalise the propagators to one at zero distance (the behaviour of the amplitudes will be discussed below) to put in evidence the decay rate as a function of euclidean time. It is immediate to notice that the glueball correlator decays much slower in the superfluid phase, indicating that the lowest excitation in the gluonic channel becomes lighter.

In the remaining part of this section we discuss first the behaviour of the amplitudes of the correlators, then we analyze their long Euclidean time behaviour. The former indicate the critical point, the latter allow a quantitative estimate of the spectrum in the two phases.

### 5.1 Amplitude

Fig. 6 shows the amplitudes  $C(0)$  of the correlators, eq. 10, as a function of the chemical potential, for the raw data,

and for a representative value of  $T_s$ . Other smeared data behave similarly. Remember that our estimates of the pion mass, as well as previous results [9], indicate  $\mu_c(m_q = 0.05) = 0.28(1)$  and  $\mu_c(m_q = 0.07) = 0.32(2)$ . We note that the amplitudes peak in correspondence with these values.

This is consistent with their definition. In fact,  $C(0)$  is defined as

$$C(0) = \frac{1}{N_t} \sum_{\tau=0}^{N_t-1} (\langle \phi^{0++}(\tau)^2 \rangle - \langle \phi^{0++}(\tau) \rangle^2) \quad (13)$$

hence, it is related with the plaquette susceptibility, which is a standard indicator of criticality.

A second observation concerns the amplitude in the superfluid phase, where the amplitude itself gets smaller.

Moreover, see again Fig. 6, which shows that the effect of the smearing becomes more pronounced in the superfluid phase. Smearing cancels ultraviolet fluctuations and preserves long distance physics. Naïvely, any observable which has only short distance components would disappear after smearing. Since in the high density phase the residual amplitudes is comparably smaller than in the low density phase, one might conclude that the relative weight of long distance, low mass components in the high density phase is comparatively smaller than in the low density phase - in other words, if the amplitudes would become zero, the glueball would decouple completely.

At even larger  $\mu$  value the results increase and approach the quenched ones, in agreement with the conclusions in ref. [25].

The main conclusion from the consideration of the amplitudes is that the either the transition and the superfluid phase are clearly seen also in a pure gluonic channel. This demonstrates the effect of a finite density of baryons on the gauge fields: since our operators do not contain explicitly the chemical potential, this dependence is only possible if the gauge field themselves are affected by a density of baryons, both in a pure phase and at the critical point.

These results indicate a sizable modification in the gluonic sector induced by a finite density of baryons. It is then very natural to ask ourselves if the confining properties of the theory are affected as well. To address this question, even at a very preliminary level, we study the behaviour of the Polyakov loop, which is an exact order parameter for confinement in the quenched theory, and an indicator of enhanced screening properties with dynamical fermions.

We show in Fig. 7 the behaviour of the Polyakov Loop at mass  $m_q = 0.05$  as a function of  $\mu$ . The effect, if any, is very modest and more visible for the spatial loop. As a comparison, we show also the spatial Polyakov loop. To attempt to put in evidence bubble or ordered structures we have also computed, and plotted in the same figure, the average of the absolute modulus of the local loops. They stay constant as well. These results suggest that the confining properties of the superfluid phase appearing at  $\mu_q > m_\pi/2$  are the same as those of the hadronic phase, in agreement with [27]. In the same paper [27] the Polyakov loop is shown to increase from near-zero values at even

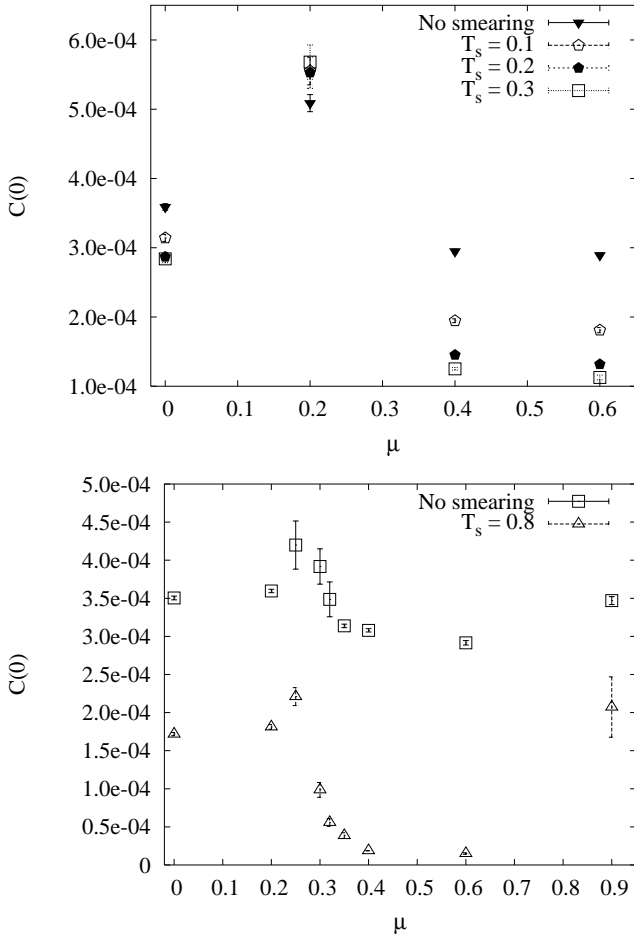


**Fig. 6.** Amplitudes of the correlator as a function of  $\mu$  for raw and smeared data, and quark mass  $m_q = 0.05(0.07)$ , upper (lower) diagram. The amplitudes, related with the plaquette susceptibilities, peak at the critical point  $\mu_c = m_\pi/2$  and decrease in the superfluid phase. These features demonstrate that the phase transition is visible in the gluonic sector, and that a high density of baryons affect the gluon mass spectrum in the superfluid phase.

larger  $\mu$ , implying that the confining property of the vacuum is lost at very high density. In this paper we only consider the BEC superfluid phase appearing at  $\mu_q > m_\pi/2$ , and we do not discuss any further transition or crossover at larger  $\mu$ .

## 5.2 Glueballs in the normal phase

The measurements of the glueballs in normal conditions are notoriously difficult, since the glueballs themselves are rather heavy. To be more specific, the plaquette correlators are basically constant within errors. To put in evidence the exponential decay one needs to subtract the long distance plateau. This is accomplished by exploiting the cluster property, and subtracting the square of the plaquette. Once this is done a signal for the mass - the value of the exponent - can be detected, while the errors

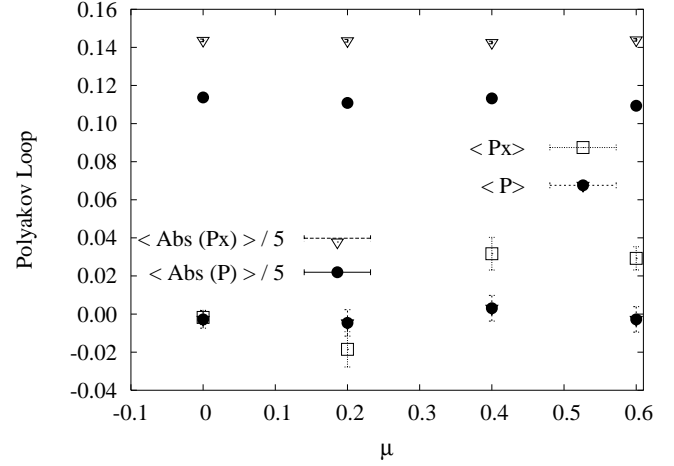


**Fig. 7.** Polyakov loop  $P$ , and spacial Polyakov loop  $P_x$  at  $m_q = 0.05$  as a function of  $\mu$ . It is also shown the (rescaled) average of the local absolute values of the same observables.

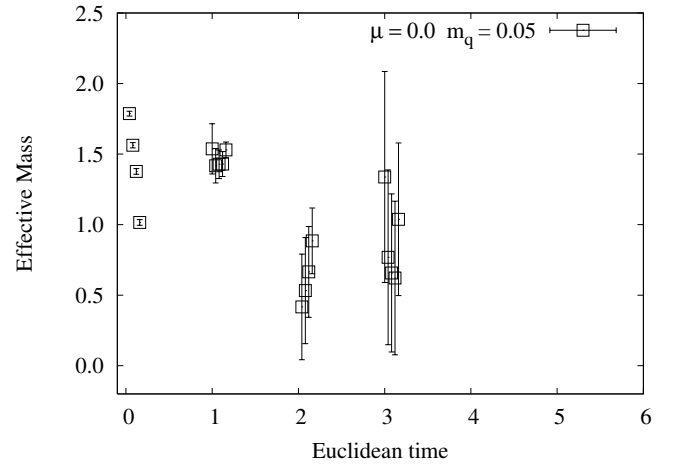


**Fig. 8.** Glueball effective masses as a function of Euclidean time, for  $\mu = 0.0$  and  $m_q = 0.05$ . Results for  $T_s = N_s \times w = 0, 0.1, 0.2, 0.3, 1.2$  are plotted slightly displaced one from the other, from left to right.

of the fits on the amplitudes remain large. This procedure is justifiable only when all of the excitations are massive, which we expect to be the case in the pure phases, while in the critical region the presence of soft, massless excitations might call for some additional care. In any case, the validity of the procedure can be assessed a posteriori from the quality of the exponential fits.

We present some results here for the sake of comparison with the analysis in the superfluid phase, which is the main goal of this study.

We have started with an effective mass analysis, where a time-dependent mass  $m_{eff}(\bar{t})$  is extracted according to eq. 5.

We have studied the smearing dependence of the effective masses extracted at different Euclidean times. The effective mass should approach the true lowest excitation

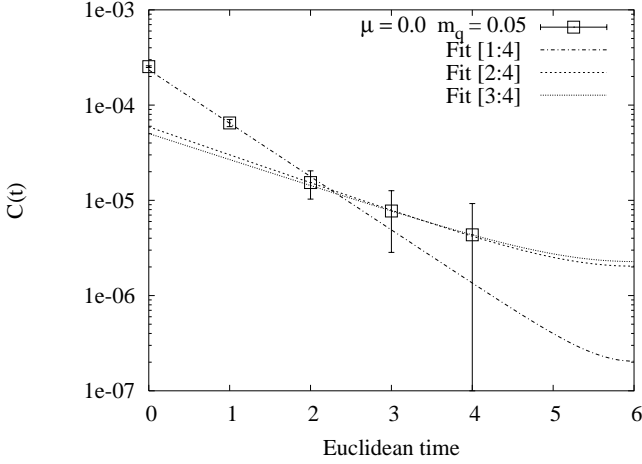


**Fig. 9.** Details of the fits for different time interval for  $\mu = 0.0$ ,  $m_q = 0.05$ , smearing weight  $w = .2$  and  $N_s = 2$  ( $T_s = 0.2$ ). Fits to propagators with other smearing parameters behave similarly, see text for details, and Table 2 for a summary of the results.

either at large  $T_s$  and/or large Euclidean time, and considering the simultaneous dependence on these parameters should in principle allow a good control on this measure.

We show the results for the effective masses extracted from correlators at  $m_q = 0.05$ , for  $T_s = 0.0, 0.1, 0.2, 0.3, 1.2$  in Fig. 8. The results are very noisy, anyway it is clear that in the normal phase the glueball is heavy as expected, and our results allow us to place at least a lower bound for its value.

Next, we performed direct fits of the data to the form of eq. 5. In attempt at improving the quality of the results we considered, along side with  $T_s = 0.6$  and  $1.2$ , two higher values of  $T_s$ .

For  $m_q = 0.05$  the fits for  $t \geq 2$  were satisfactory, while those including  $t = 1$  were not adequate to describe the largest time distances, as apparent also from a higher  $\chi^2$ . As an example, in Fig. 9 we show some fits for the parameters  $w=0.2$  and  $N_s = 2$  ( $T_s = 0.4$ ). The resulting masses where  $1.32(2)$  for the fit performed in the time interval  $[1:4]$ , which is clearly missing the large time separation behaviour, while the fits in the interval  $[2:4]$ , and  $[3:4]$  gives  $0.68$  and  $0.63$ , in good agreement with each other, but errors on the fit can be hardly estimated, given the large errors on the propagators themselves. The behaviour demonstrated in Fig. 9 is generic for the  $m_q = 0.05$ , and for  $T_s = .6$  and  $1.2$  for  $m_q = 0.07$ .

For the two larger values of  $T_s$  which we have considered,  $T_s = 1.6$  and  $T_s = 2.0$  the fit of propagators with a larger  $T_s$  in the interval  $[2:5]$  are of a poor quality, while the fits in the interval  $[1:5]$  offer a good description of the data, in agreement with results at smaller  $T_s$ , for  $t \geq 2$ . In most cases the propagators for Euclidean time 5 and 6 where zero within errors, as expected given the large values of the mass, and including them does not change the quality of the fits.

**Table 2.** Results for the  $0^{++}$  Glueball at  $\mu = 0$

$m_q = 0.05$				
	$T_s = .6$	$T_s = 1.2$	$T_s = 1.6$	$T_s = 2.0$
$m$	0.85(12)	0.98(12)	1.02(12)	1.05(12)
$\chi^2$	0.08	0.08	0.08	0.08
$m_q = 0.07$				
	$T_s = .6$	$T_s = 1.2$	$T_s = 1.6$	$T_s = 2.0$
$m$	1.02(8)	1.7(4)	2.05(8)	2.08(8)
$\chi^2$	1.93	0.2	0.2	0.2

**Table 3.** Results for the  $0^{++}$  Glueball at  $\mu = 0$  from fits with an open vacuum contribution.

Time interval [2:4]				
	$T_s = .6$	$T_s = 1.2$	$T_s = 1.6$	$T_s = 2.0$
$m$	0.93	0.82	0.84	0.89
Time interval [2:5]				
	$T_s = .6$	$T_s = 1.2$	$T_s = 1.6$	$T_s = 2.0$
$m$	0.4(4)	0.62(25)	0.68(12)	0.73(11)

We summarize the results from the fits at  $\mu = 0$  in Table 2. For  $m_q = 0.05$ , and all  $T_s$ , we quote results and errors from the fits in the  $[2:4]$  interval.

For  $m_q = 0.07$ , a direct comparison of the results show that the glueball masses are indeed heavier than those at  $m_q = 0.05$ . This implies that the propagators at  $m_q = 0.07$  can be compatible with zero already at a distance 4, and when this happens is very difficult to obtain reliable estimates. For  $T_s = 0.6, 1.2$  we quote the results obtained by fitting data in the  $[2,5]$  interval. They are consistent with those in the  $[3,5]$  interval, which have however a lower significance. For two higher  $T_s$  values we quote the results of the fits in the  $[1,5]$  interval (the results in the  $[2,5]$  interval are  $m = 2.03(50)$ , and  $m = 2.24(65)$ , compatible in the large errors), having in mind that these might well represent upper bounds rather than asymptotic estimates.

Finally, we consider also the plaquette correlators eq. 12 where the vacuum contribution was left as a fitting parameter. To compare the two fitting forms we considered first the same fitting interval  $[2:4]$ , as well as an extended to interval  $[2:5]$ , and we show the results for  $m_q = 0.05$  in Table 3, while Fig. 10 illustrates the generic features of the results. All in all, subtracting the background allows to constrain one parameter fit to zero, thus achieving a more precise fit, but the results within the larger errors are in substantial agreement. In particular, the fitted vacuum coincides with its direct calculation.

### 5.3 Glueballs in the superfluid phase

We have first performed an effective mass analysis. We show in Fig. 11 a subset of the results, for quark mass  $m = 0.05$ , and  $\mu = 0.6$ , and selected values of  $T_s$ .  $\mu = 0.06$  is well below the saturation threshold, the baryonic density is less than one (see e.g. [24]) and the results for the amplitudes are far from the quenched ones, which are approached only when  $\mu$  approaches 0.9, as discussed above.



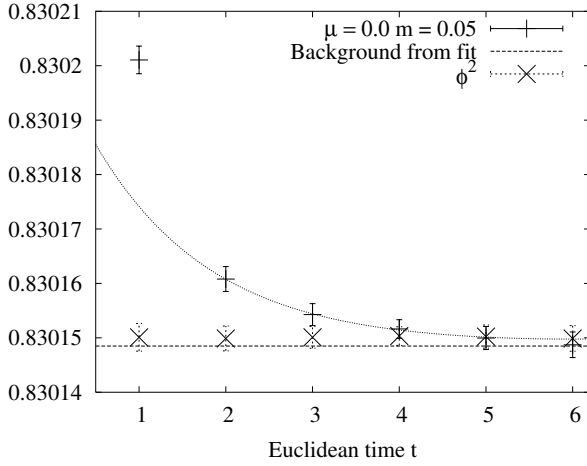


**Fig. 10.** Fit of the plaquette correlator,  $m_q = 0.05$ ,  $\mu = 0.0$ ,  $T_s = 2.0$ . The mass value is consistent with the estimate from the effective mass analysis and the fits with subtracted background and the fitted vacuum coincide with errors with the fitted measurement.

At a variance with the behaviour observed at  $\mu = 0.0$ , here a plateau begins to emerge, indicating that by increasing the time distance, and/or the number of smearing steps we can approach the asymptotic behaviour representing the true value of the mass.

The fits proven to be rather stable, and indeed we observed convergence over a rather large interval of  $T_s$ , the convergence to the final results being faster in the time interval  $[1 : 5]$ . We underscore that for  $t = 5$  the signal is very weak, so the interval  $[1 : 5]$  is the smallest which can be fitted in a meaningful way. We summarise the results for the masses over a large set of  $T_s$  in Fig. 12, which demonstrates the nice convergence of the results. The effective mass analysis give also compatible results, within the larger errors.

Finally, Table 4 collects the results for the glueball masses obtained for the fits with  $\mu \neq 0$ .

Also in this case we performed fits with an open vacuum contribution, choosing the same interval  $[1:5]$  where the results of the standard fits proven to be stable with increasing smearing parameter  $T_s$ , and in good agreement with effective masses estimates.

The quality of the fits was very good, however the mass results turned out to be larger than those obtained by fitting the propagator with the subtracted vacuum contribution. In addition to this, the fitted vacuum was definitively much larger than the direct measurement. Since the fitted mass was rather large, we should expect not only the agreement between fitted vacuum and direct estimate, but also an asymptotic behaviour of the propagator reaching a plateau given by such a common value, see Fig. 13, top.

This is not what we are observing: the plaquette correlator levels off at a value which is much higher than the direct estimate of the vacuum contribution. This behaviour can be explained by a contribution from a light mass which is obscured by the background.

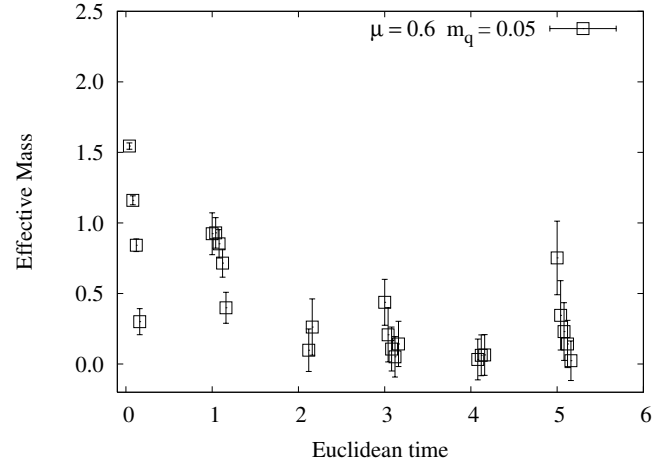


**Fig. 11.** Glueball effective masses as a function of Euclidean time, for  $\mu = 0.6$  and  $m_q = 0.05$ . Results for  $T_s = N_s \times w = 0, 0.1, 0.2, 0.3, 1.2$  are plotted slightly displaced one from the other, for increasing values of  $T_s$ .

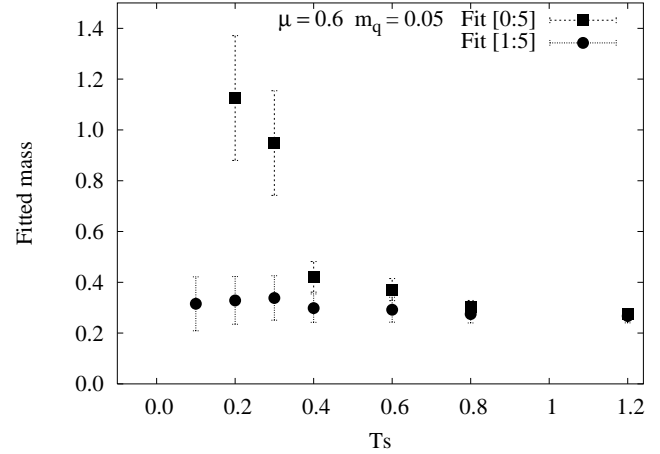


**Fig. 12.** Fit results as a function of the smearing parameter, for the two interval considered. The results confirm the ones seen in the effective masses, with smaller errors

To shed light on these observations we performed further fits this time using a constrained value of the mass equal to the one coming from the fits with the subtracted vacuum contribution. In those cases we obtained acceptable results, with the correct value of the vacuum contribution, see Fig 13, bottom.

A tentative conclusion is thus that it is difficult to disentangle the contribution from a low mass excitation from an extra contribution to the background. To exhibit the correct behaviour we have to constrain the background to the measured value. If we do so, either the effective mass analysis and the standard fits produce results consistent with each other, over a large set of smearing parameters and two different time intervals.

Clearly to confirm this picture we should repeat our measurements on lattices more elongated, and with a larger size. If the picture outlined here is correct, on a larger lat-

**Table 4.** Glueball masses at  $\mu \neq 0$  extracted from different fits

m = 0.05				
	$T_s = .6$	$T_s = 1.2$	$T_s = 1.6$	$T_s = 2.0$
$\mu = .2$	-	-	-	-
$\mu = .4$	-	1.34 (6)	1.16(4)	1.07(4)
$\mu = .6$	0.31(8)	0.27(3)	0.26(2)	0.27(2)
Reduced $\chi^2$ associated to the fits above				
	$T_s = .6$	$T_s = 1.2$	$T_s = 1.6$	$T_s = 2.0$
$\mu = .2$	-	-	-	-
$\mu = .4$	-	0.6	0.37	0.30
$\mu = .6$	1.2	0.22	0.16	0.14

m = 0.07				
	$T_s = .6$	$T_s = 1.2$	$T_s = 1.6$	$T_s = 2.0$
$\mu = .2$	2.02(38)	2.05(28)	2.06(24)	2.05(27)
$\mu = .4$	-	1.29 (34)	1.40(4)	1.15(7)
$\mu = .6$	0.41(8)	0.35(4)	0.35(3)	0.35(3)
Reduced $\chi^2$ associated to the fits above				
	$T_s = .6$	$T_s = 1.2$	$T_s = 1.6$	$T_s = 2.0$
$\mu = .2$	1.73	2.77	2.13	1.73
$\mu = .4$	-	1.18	0.03	0.17
$\mu = .6$	2.36	1.06	0.82	0.78

**Table 5.** Glueball masses at  $\mu = 0.6$  extracted from different fits with an open vacuum contribution

m = 0.05				
	$T_s = .6$	$T_s = 1.2$	$T_s = 1.6$	$T_s = 2.0$
$\mu = .6$	1.73(1)	1.00(5)	0.89(5)	0.84(6)
Reduced $\chi^2$ associated to the fits above				
	$T_s = .6$	$T_s = 1.2$	$T_s = 1.6$	$T_s = 2.0$
$\mu = .6$	0.00001	0.027	0.03	0.05

m = 0.07				
	$T_s = .6$	$T_s = 1.2$	$T_s = 1.6$	$T_s = 2.0$
$\mu = .6$	1.55(10)	1.19(7)	0.89(6)	0.85(6)
Reduced $\chi^2$ associated to the fits above				
	$T_s = .6$	$T_s = 1.2$	$T_s = 1.6$	$T_s = 2.0$
$\mu = .6$	0.02	0.02	0.03	0.03

tice we should be able to measure a two state signal, and to observe with confidence an asymptotic behaviour, stable over several smearing steps.

#### 5.4 The critical region

As mentioned at the beginning of this Section, the critical propagators show a puzzling feature, namely the square of the plaquette turns out to be larger than the minimum of the propagator itself: if we subtract it, as done in the pure phases, the propagator would become negative [31].

It is rather natural to interpret this behaviour as the manifestation of massless modes, which develop at the phase transition. In the presence of massless excitations there is no reason to expect a plateau in the propagators, so the negative region which would emerge subtracting the square of the plaquette has no particular significance.

On the other hand, it is clear that a finite lattice cannot accomodate such massless excitations. We only know

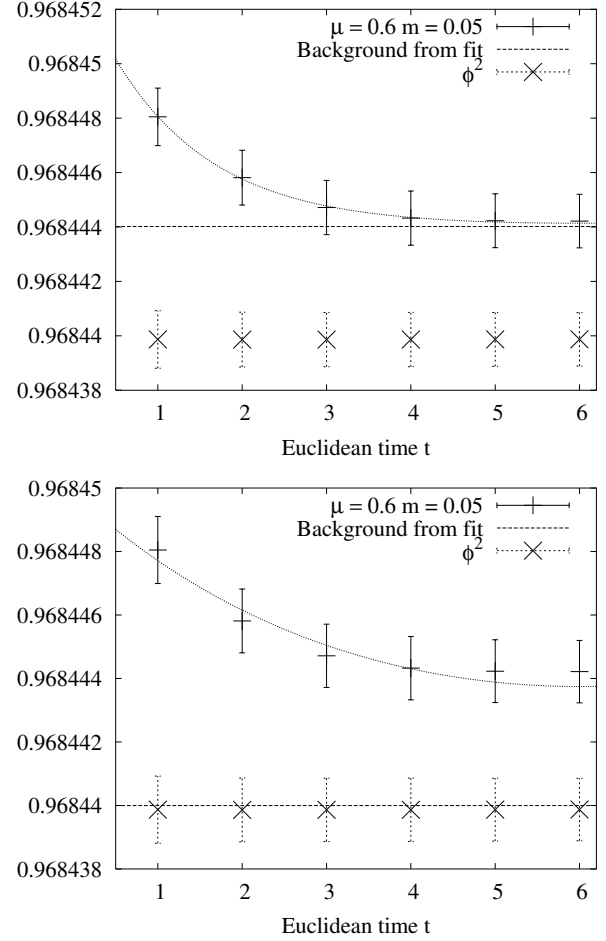


**Fig. 13.** The plaquette correlator at  $m_q = 0.05$ ,  $\mu = 0.6$ ,  $T_s = 2.0$  with superimposed the fit with an open background. The fitted value of the vacuum contribution and its direct measurement are shown as well, demonstrating a mismatch and an overall inconsistency of this fit (top). The same, but with the mass value constrained to that measured in the fit with a subtracted background. The quality of the fit is poorer, but this time there are no inconsistencies (bottom)

that the propagator should become periodical, and it is reasonable to assume that it should be continuous with all its derivatives at the origin, since there is no discrete spectrum dominating the short distance behaviour. These considerations suggest to try fits with three parameters  $a, b, c$  of the form:

$$C(t) = a \cos(2\pi t/N_t) \cosh[b(t - N_t/2)] + c \quad (14)$$

We show in Fig. 14 these fits for the raw data, and for the smeared ones. The stability of the results is excellent, note in particular that the fit in the restricted interval  $[3 : 6]$  describes perfectly the data at smaller time distance, including zero for the smeared results, where the ultraviolet fluctuations are suppressed.

In this picture the glueball propagator in the critical region has two complex conjugates poles, whose imaginary

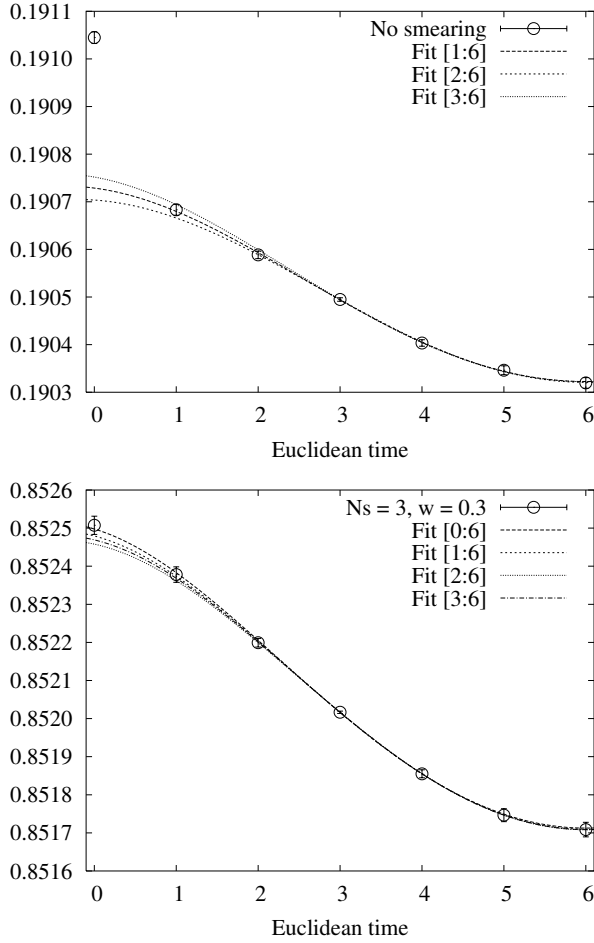


**Fig. 14.** The propagator at  $m_q = 0.05$ , and  $\mu = 0.2 \simeq \mu_c$ , with superimposed the fits described in the text. The raw (smeared) data are shown in the top (bottom) diagram. We obtain excellent fits to a damped oscillation with period  $N_t$ , note in particular the smeared results where a fit constrained to the interval [3:6] successfully describes the data in the entire interval

part  $2\pi/N_t$  goes to zero in the thermodynamic limit. It is clear that only a combined finite size and finite  $N_t$  scaling analysis both in the spacial and in the temporal direction might confirm or disprove this interpretation.

## 6 Summary and discussions

We have studied the gluodynamics of two color QCD at very low temperature, and nonzero chemical potential.

We have noted that the Polyakov loop is nearly insensitive to the transition from the hadronic to the superfluid phase, in agreement with the observations of [27], and suggesting that the superfluid phase shares the same confining properties as the hadronic phase in a rather large interval of chemical potential. We have not addressed the possibility of a deconfining transition taking place at an even larger  $\mu$  value and the possibility of a BEC/BCS crossover discussed in [27].

We have observed a gluonic transition - signaled by a peak of the plaquette susceptibility - coincident with the superfluid transition at  $\mu_c = m_\pi/2$ . Beyond this transition, in the superfluid phase, the susceptibility reaches a lower value than in the normal phase.

We have studied the scalar glueball propagator in the normal and in the superfluid phase. In both phases the propagators are amenable to standard hyperbolic cosine fits, and related effective mass analysis. In the normal phase the results from two different fits - one with a subtracted vacuum contribution, and the other with the vacuum contribution left as a free parameter - give results in good agreement one with another. In the superfluid phase the subtraction of the background seems mandatory to obtain coherent results, and in this case it turns out that the lightest excitation in the scalar glueball channel is lighter by about a factor two in the superfluid phase than in the normal phase. The fit with a free background would produce a larger mass, but also an anomalously large fitted value for the vacuum contribution, not compatible with the direct calculations.

At the present stage, we can conclude that our results indicate a non trivial modification of the gluonic vacuum in the low temperature, superfluid phase.

To put the above considerations on firmer quantitative grounds we would need simulations on a larger and more elongated lattice, as well as a careful considerations of the mixing effects with fermionic channels with the same quantum numbers.

One interesting open question concerns the mass dependence of the results. We already know that in the large chemical potential limit, beyond the saturation threshold, we recover the quenched behaviour [25]. The quenched limit is also obtained at infinite mass, and in that case the gluon fields should not be sensitive to the chemical potential. Then, when increasing the mass, the critical point would move forward and forward, eventually collapsing with the saturation threshold at infinite mass, in which case all gluonic observables will remain constant and equal their  $\mu = 0$  value. This suggests the possible existence of an endpoint of the transition in the chemical potential mass plane, which will be interesting to explore.

One final comment concerns the interrelation, or lack thereof, of these studies with real QCD. Following a large  $N_c$  analysis it was proposed [38] that the matter immediately above  $\mu_c$  is “quarkyonic” - the authors chose this name to indicate a phase with an unusual realization of chiral symmetry, which still remains confining. This phase, according to the authors, should persist till relatively large temperatures, and should not break color symmetry, at variance with the ordinary superconducting or CFL phases which are indeed features of the very low temperatures, and which break color symmetry. The two scenarios of the large  $N_c$  a quarkyonic phase and the small  $N_c$  superfluid phase share a few common aspects: they are confining, with unusual realization of chiral symmetry, do not break color symmetry and should persist till relatively large temperature. The physical phase diagram of real QCD at low temperatures should in some sense interpolate between

the two. It is tempting to regard the superfluid phase as a limiting case of the quarkyonic phase of large  $N_c$  QCD. Should this be true, two color QCD might be a better guidance to the understanding of the QCD phase diagram in the physical case than previously thought.

## Acknowledgments

We wish to thank A. E. Dorokhov, S. J. Hands, E. M. Ilgenfritz, M. Müller-Preussker, D. T. Son and M. Testa for helpful conversations. MPL thanks the D.o.E Institute for Nuclear Theory at the University of Washington for its hospitality during the completion of this work. The simulations were performed on the ATLAS computer farm in Rome and we thank A. De Salvo for his invaluable help during the development of this high statistics project.

## References

1. M. G. Alford, A. Schmitt, K. Rajagopal and T. Schafer, arXiv:0709.4635 [hep-ph] and references therein
2. M. A. Stephanov, PoS **LAT2006** (2006) 024 [arXiv:hep-lat/0701002].
3. D. K. Sinclair, J. B. Kogut and D. Toublan, Prog. Theor. Phys. Suppl. **153** (2004) 40 [arXiv:hep-lat/0311019].
4. J. B. Kogut, H. Matsuoka, M. Stone, H. W. Wyld, S. H. Shenker, J. Shigemitsu and D. K. Sinclair, Nucl. Phys. B **225** (1983) 93.
5. A. Nakamura, Phys. Lett. B **149** (1984) 391.
6. E. Dagotto, F. Karsch and A. Moreo, Phys. Lett. B **169** (1986) 421.
7. M. G. Alford, K. Rajagopal and F. Wilczek, Phys. Lett. B **422**, 247 (1998) [arXiv:hep-ph/9711395].
8. R. Rapp, T. Schafer, E. V. Shuryak and M. Velkovsky, Phys. Rev. Lett. **81**, 53 (1998) [arXiv:hep-ph/9711396].
9. S. Hands, J. B. Kogut, M. P. Lombardo and S. E. Morrison, Nucl. Phys. B **558**, 327 (1999) [arXiv:hep-lat/9902034].
10. J. B. Kogut, D. K. Sinclair, S. J. Hands and S. E. Morrison, Phys. Rev. D **64**, 094505 (2001) [arXiv:hep-lat/0105026].
11. R. Aloisio, V. Azcoiti, G. Di Carlo, A. Galante and A. F. Grillo, Nucl. Phys. B **606**, 322 (2001) [arXiv:hep-lat/0011079].
12. G. Akemann, J. C. Osborn, K. Splittorff and J. J. M. Verbaarschot, Nucl. Phys. B **712**, 287 (2005) [arXiv:hep-th/0411030].
13. K. Splittorff and J. J. M. Verbaarschot, Prog. Theor. Phys. Suppl. **168** (2007) 265, and references therein.
14. E. Bittner, M. P. Lombardo, H. Markum and R. Pülirsch, Nucl. Phys. Proc. Suppl. **94** (2001) 445 [arXiv:hep-lat/0010018].
15. J. B. Kogut, M. A. Stephanov, D. Toublan, J. J. M. Verbaarschot and A. Zhitnitsky, Nucl. Phys. B **582** (2000) 477 [arXiv:hep-ph/0001171].
16. A. Zhitnitsky, AIP Conf. Proc. **892** (2007) 518 [arXiv:hep-ph/0701065].
17. F. Sannino and K. Tuominen, Phys. Rev. D **70** (2004) 034019 [arXiv:hep-ph/0403175].
18. S. Chandrasekharan and F. J. Jiang, Phys. Rev. D **74** (2006) 014506 [arXiv:hep-lat/0602031].
19. F. Sannino, Phys. Rev. D **67** (2003) 054006; F. Sannino, AIP Conf. Proc. **688** (2004) 121 [arXiv:hep-ph/0307053], and references therein.
20. B. Alles, M. D'Elia, M. P. Lombardo and M. Pepe, in *Quark Gluon Plasma and Relativistic Heavy Ions*, World Scientific Publishing, Singapore, 2002, p. 271.
21. S. Muroya, A. Nakamura and C. Nonaka, Phys. Lett. B **551** (2003) 305 [arXiv:hep-lat/0211010].
22. S. J. Hands and C. G. Strouthos, arXiv:hep-lat/0408007, published in K. J. Eskola et al. (Ed.) *Strong and Electroweak Matter*, World Scientific Publishing, Singapore, 2004, p.431.
23. S. Hands, P. Sitch and J. I. Skullerud, arXiv:0710.1966 [hep-lat].
24. M. P. Lombardo, arXiv:hep-lat/9907025.
25. B. Alles, M. D'Elia and M. P. Lombardo, Nucl. Phys. B **752** (2006) 124 [arXiv:hep-lat/0602022].
26. S. Conradi, A. D'Alessandro and M. D'Elia, Phys. Rev. D **76** (2007) 054504 [arXiv:0705.3698 [hep-lat]].
27. S. Hands, S. Kim and J. I. Skullerud, Eur. Phys. J. C **48** (2006) 193 [arXiv:hep-lat/0604004].
28. N. Ishii, H. Suganuma and H. Matsufuru, Phys. Rev. D **66** (2002) 094506
29. N. Ishii, H. Suganuma and H. Matsufuru, Phys. Rev. D **66** (2002) 014507
30. M. P. Lombardo, M. L. Paciello, S. Petrarca and B. Taglienti, Nucl. Phys. Proc. Suppl. **129** (2004) 635 [arXiv:hep-lat/0309110].
31. M. P. Lombardo, M. L. Paciello, S. Petrarca and B. Taglienti, PoS **LAT2007** [arXiv:0710.3251 [hep-lat]].
32. P. Hasenfratz and F. Karsch, Phys. Lett. B **125** (1983) 308.
33. M. Falcioni, M. L. Paciello, G. Parisi and B. Taglienti, Nucl. Phys. B **251**[FS13] (1985) 624.
34. M. Albanese *et al.* [APE Collaboration], Phys. Lett. B **192** (1987) 163; M. Albanese *et al.* [APE Collaboration], Phys. Lett. B **197** (1987) 400.
35. F. D. R. Bonnet, P. Fitzhenry, D. B. Leinweber, M. R. Stanford and A. G. Williams, Phys. Rev. D **62** (2000) 094509
36. R. Gupta, A. Patel, C. F. Baillie, G. W. Kilcup and S. R. Sharpe, Phys. Rev. D **43** (1991) 2301.
37. L. Giusti, M. L. Paciello, C. Parrinello, S. Petrarca and B. Taglienti, Int. J. Mod. Phys. A **16** (2001) 3487
38. L. McLerran and R. D. Pisarski, Nucl. Phys. A **796**, 83 (2007) [arXiv:0706.2191 [hep-ph]].

